Oceanologia (2015) 57, 132—143

Available online at www.sciencedirect.com

ScienceDirect

journal homepage: www.elsevier.com/locate/oceano

ORIGINAL RESEARCH ARTICLE

Variability of currents over the southern slope of the Gulf of Finland☆

Irina Suhhova*, **Juss Pavelson**, **Priidik Lagemaa**

Marine Systems Institute at Tallinn University of Technology, Tallinn, Estonia

Received 27 November 2014; accepted 19 January 2015
Available online 29 January 2015

KEYWORDS
Slope current;
Stratification;
Up-/downwelling;
The Gulf of Finland

Summary In our intraseasonal variability studies of currents in the coastal sea of the Gulf of Finland northeast of Pakri Peninsula, we compared the observation data from a bottom-mounted ADCP (March—June of 2009, 50 m depth) with the simulation data from High Resolution Operational Model of the Baltic (HIROMB). The structure of the current pattern appeared strongly dependent on the stratification conditions. The flow was quasi-barotropic during the periods of weak inverse thermal stratification at the end of winter season and at transition from the inverse thermal stratification to summer type stratification when the sea was thermally unstratified, but mostly two-layered (baroclinic) when the summer type thermal stratification had developed. The alternation of strong westward (eastward) currents (up to 30 cm s^{-1}) in the upper layer is explained in terms of coastal upwelling (downwelling) due to favourable background winds. The measured and the modelled upper layers along isobath currents showed a noticeable correlation with the correlation coefficient of 0.52 and 0.82 during the periods of winter type and summer type stratifications, respectively, and the absence of a significant correlation during the transition period. The eastward (upwind) current episodes with speeds reaching 18 cm s^{-1} below the seasonal thermocline are likely to reflect the specific circulation response in the elongated basin caused by the easterly wind. The long-term mean (over 3.5 months) current vector (−2.0 cm s^{-1}, −2.9 cm s^{-1}) was westward in the upper sea and eastward, nearly along isobaths (1.1 cm s^{-1}, −0.3 cm s^{-1}) in the deeper layers.

☆ This study was supported by the Estonian Science Foundation Grant 9381 and institutional research funding IUT19-6 of the Estonian Ministry of Education and Research.
* Corresponding author at: Marine Systems Institute at Tallinn University of Technology, Akadeemia tee 15A, 12618 Tallinn, Estonia. Tel.: +372 6204309.
E-mail address: irina.suhhova@msi.ttu.ee (I. Suhhova).
Peer review under the responsibility of Institute of Oceanology of the Polish Academy of Sciences.

ELSEVIER Production and hosting by Elsevier

http://dx.doi.org/10.1016/j.oceano.2015.01.001

1. Introduction

Currents along the continental slope of oceans have been widely studied. Basically, the topographic steering mechanism favours the location of strong flow along the slope, while their maintenance, character, and cross-shelf distribution depend on different forcing factors. Freshwater runoff, along-shore pressure gradient and steady along-shelf wind stress are known as main agents to support coastal currents (e.g., Huthnance, 1995). Similarly, slope currents have been frequently examined in smaller water bodies like the Adriatic Sea (Cushman-Roisin et al., 2001) and the Great Lakes (Rao and Schwab, 2007). At the same time, observational evidence of the current structure along the slopes of the Gulf of Finland, known as the second largest sub-basin of the Baltic Sea, is scarce. Therefore, the objective of the present study is to diminish this gap by using current measurements of a few months' duration at a single site on the southern slope of the western Gulf of Finland.

The Gulf of Finland (Fig. 1a), a relatively shallow and elongated estuarine-like basin, lies in the northeastern part of the tideless Baltic Sea. The gulf is about 400 km long, its width varies between 48 km and 135 km and its total volume is ~1100 km^3. The along-axis depth of the gulf decreases almost monotonically from 80 to 110 m at its entrance to 20—30 m in the eastern part. The coastline and bottom topography as a whole are complex; in the western gulf, a gentle slope on the northern coast and rather steep slope on the southern coast separate the shallow coastal sea from the deep gulf. The long-term mean circulation in the Gulf of Finland is weak and cyclonic, as evidenced by observations (Alenius et al., 1998; Soomere et al., 2008) as well as by the simulations of numerical models (Andrejev et al., 2004; Elken et al., 2011). Such a mean flow scheme is to a large extent caused by the freshwater discharge of the large Neva River (annual runoff ~110 km^3) in the eastern end of the gulf. As a consequence, the buoyancy-driven Finnish Coastal Current quasi-permanently carries the fresher water westward (Stipa, 2004). In the Estonian coastal sea, an eastward flow of the northern Baltic Proper saltier water is commonly expected. In addition, in the upper layer, pronounced gyre-like currents related to different sub-basins of the gulf are found (Elken et al., 2011; Lagemaa, 2012). At shorter time-scales, the current system is often more complicated and evidently depends on wind variations. The wind field over the Baltic Sea is influenced by the mostly eastward moving atmospheric cyclones. In the northern Baltic Proper and the western Gulf of Finland, the S-W and to a lesser extent the E winds dominate (Soomere and Keevalik, 2003), which are favourable for forcing coastal up- and downwelling. These wind-forced events are usually accompanied by the strong coastal jet-like currents (Laanemets et al., 2005; Suursaar and Aps, 2007; Zhurbas et al., 2008).

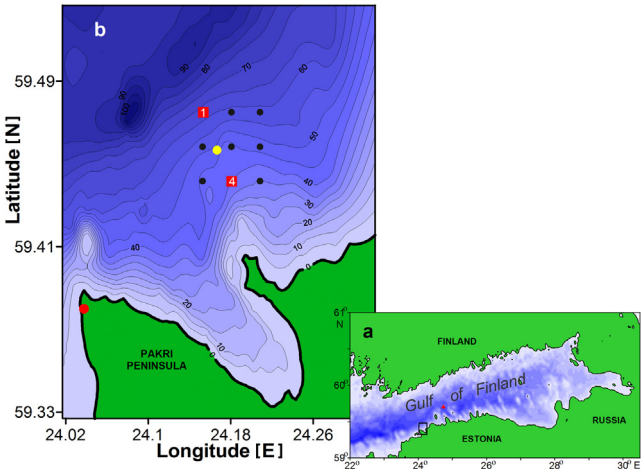

Figure 1 (a) Map of the Gulf of Finland. The study area is indicated by a rectangle and the Tallinnamadal Lighthouse weather station by a red triangle. (b) Bathymetric map of the study area. The location of the bottom-mounted ADCP is shown by a yellow dot and the Pakri weather station by a red dot. Black dots and red squares with labels mark the grid points of the HIROMB model from which data were used. Data from grid point 3 were used for comparison with the ADCP data. Across-isobaths sea level gradients were calculated using data from grid points 1 and 4. Such choice of grid points gives nearly the same rotation of axes (27°) as for the current velocity (30°). (For interpretation of the references to colour in this figure legend, the reader is referred to the web version of this article.)

The thermal stratification in the upper gulf has a highly seasonal character (Alenius et al., 1998). By the end of winter season, the water body is characterised by relatively weak inverse thermal stratification with a temperature increase from about 0°C by the sea surface to about 4°C in the depth. The solar heating and wind mixing form a sharp seasonal thermocline/pycnocline starting from May, and in summer it is centred at the depth of 10—15 m (Liblik and Lips, 2011). The haline stratification has weaker seasonality, but changes largely along the gulf because of the Neva River runoff. In the western gulf, as the continuation of the Baltic Proper, a permanent halocline with the salinity difference of 2—3 psu is located at the depth of about 60—70 m. Also, short-term weakening of haline stratification is possible due to the reverse of ordinary estuarine circulation in stronger SW wind conditions (Elken et al., 2003).

In this study, we examine the structure and intraseasonal variability of current over the slope at the north-west coast of Estonia. The questions to be answered are:

(A) To which extent do the mesoscale (local) coastal processes, e.g., the upwelling/downwelling, modulate the flow?
(B) To which extent can the locally-observed flow variability be simulated by high-resolution numerical models?
(C) Is the flow mainly eastward, as expected from the estuarine type general circulation scheme of the Gulf of Finland?

The current velocity measurement period (March—June) is long enough to track the different mesoscale processes (time scale about a week) and its timing enables different stratification conditions. We focus on the forcing factors (wind, sea level) responsible for the nature and variation of the currents. The observational data are combined with hourly forecasts from the operational Baltic Sea circulation model HIROMB-SMHI to include additional parameters (stratification, sea level gradients) and to get some insight to a wider area. The paper is organised as follows. Section 2 presents

the observational data used and a brief model description. Section 3 analyses an overall variability of currents with emphasis on the flow regime during up- and downwelling events and compares the data with the model. Section 4 discusses the main findings and presents the conclusions.

2. Data and model

2.1. The ADCP data

Current velocity measurements were carried out at the southern coast of the Gulf of Finland, northeast of the Pakri Peninsula (59°27.4′N, 24°10.0′E) from 13 March to 30 June 2009 (Fig. 1b). In this region of the gulf, the bottom slope is nearly uniform and follows well the coastline. The observation site (50 m depth) is located about 6 km from the coast, i.e., practically in the central part of the slope. The deeper isobaths (>50 m) in the surrounding area are oriented in the direction of approximately 60° from the north, while the shallower ones follow more the complex coastline.

We used a 307.2 kHz broadband ADCP (Workhorse Sentinel, RD Instruments) deployed onto the bottom with a trawl-resistant platform Barnacle 60P. The instrument measured current velocity profiles over 2-m depth bins with the sampling interval of 10 min (average of 50 pings). The two first subsurface bins were truncated from the dataset as contaminated by the surface side lobe effect (∼3 m). The quality of the data at each level was then checked using the procedure developed by Book et al. (2007), which is based on certain criteria for the internal quality parameters of the ADCP (error velocity, percentage good, signal correlation). Relying on this analysis, the data from the third upper bin were found partly corrupted (more likely due to sea level variations) and were therefore removed. Thus, the current velocities were available from the depth range between the bins centred at the depths of 6.6 and 44.6 m. The data from the ADCP's pressure sensor were used to estimate the sea level changes. For the assessment of near-bottom water masses, the data from the instrument's temperature sensor (0.6 m above the bottom) were used.

2.2. Wind and sea level data

The wind data were available from the Pakri weather station (59°23.4′N, 24°02.4′E; at 33 m height) and the Tallinnamadal Lighthouse (59°42.7′N, 24°43.9′E; at 31 m height). The former is located at the tip of the Pakri Peninsula, approximately 10 km SW of the ADCP site. The Tallinnamadal Lighthouse is located farther (42 km NE), but represents the open sea wind. Comparison of hourly wind vector series from both stations revealed a good correlation (magnitude of the complex correlation coefficient $R = 0.87$) with a negligible average phase ($\Phi \approx 4°$) and lag. This shows that at both stations the wind patterns were quite similar, as might be expected considering the scale of atmospheric cyclones of a few hundred kilometres. However, the mean wind speed at Tallinnamadal was 2.6 m s^{-1} higher than at Pakri, which is likely to reflect the difference between the strength of winds measured above the open sea and mainland. Similar results were obtained by the thorough analysis of sea-measured and land-measured winds with respect to the HIRLAM (High Resolution Limited Area Model) wind in the same region of the gulf (Keevallik and Soomere, 2010; Keevallik et al., 2010). It was shown that the measured wind speed at Pakri was significantly lower than the speed from the model forecast, while the speeds from the measurements and the forecast at Tallinnamadal were approximately the same. Considering the above arguments, wind data from Tallinnamadal (5 min sampling interval) were used in the present analysis. As the wind was measured at a height of 31 m, its speed was then converted to the speed at the standard 10 m height level for the calculation of wind stress. For that purpose, the logarithmic wind speed profile was applied (Thuillier and Lappe, 1964).

Observational sea level data (1-h interval) from Pakri gauge were involved to verify the ADCP's pressure record in use as a 'sea level' at the measurement site. The contribution from the atmospheric pressure in the ADCP's hourly pressure time-series was removed using the calculated inverse barometric correction. The corrected ADCP pressure data appeared in high correlation with the Pakri sea level data (correlation coefficient $r = 0.97$) collected 10 km apart.

Current, wind, and ADCP's sea level time-series were filtered with a 1-h moving average filter and decimated to obtain hourly values for some descriptive and analysis purposes. For the low-frequency analysis, all series were filtered with a 36-h cutoff Butterworth (1930) filter. Such low-pass filter window was chosen to remove the inertial currents (period 13.9 h), seiche-driven currents with possible periods in the Gulf of Finland up to 31 h (Lilover et al., 2011), as well as other high frequency flow components. An inevitable negative effect of such filtering of the currents and winds is that it will remove some impact of storm and wind forcing from the analysis (e.g., the ocean response to the quickly moving eastward atmospheric cyclones will be more affected than the response to the more sedentary atmospheric anticyclones). Current and wind velocity vectors were rotated counterclockwise by 30° for along- and across-isobath components.

2.3. The model

A state-of-the-art circulation model HIROMB (High Resolution Operational Model for the Baltic Sea) (Funkquist, 2001) is in operational use in Estonia and therefore was used to obtain additional/background data for the analysis of the observed currents. The model with a horizontal grid step of one nautical mile (1.852 km) is run at the Swedish Meteorological and Hydrological Institute (SMHI) and forced by the atmospheric model HIRLAM (SMHI), with a grid step of 22 km. In vertical, the model has a grid step of 4 m between the surface and 12 m, 6 m between 12 m and 30 m, 10 m between 30 m and 60 m and 15 m between 60 m and 90 m. In spite of poor vertical resolution, this model has proved to have a good prediction capability of the sea level (Gästgifvars et al., 2008) and has enabled quite reasonable forecasts of flow in different parts of the Gulf of Finland (Lagemaa et al., 2010). The model includes wind drag coefficient that depends on atmospheric stability (Elken et al., 2011) and the replacement of the Successive Corrections data assimilation scheme by the Optimal Interpolation method (Lagemaa et al., 2010). The HIROMB model used in this study includes assimilation of OSI-SAF SST, Ice, MARNET buoys, in situ measurements from ships and FerryBox for salinity and temperature.

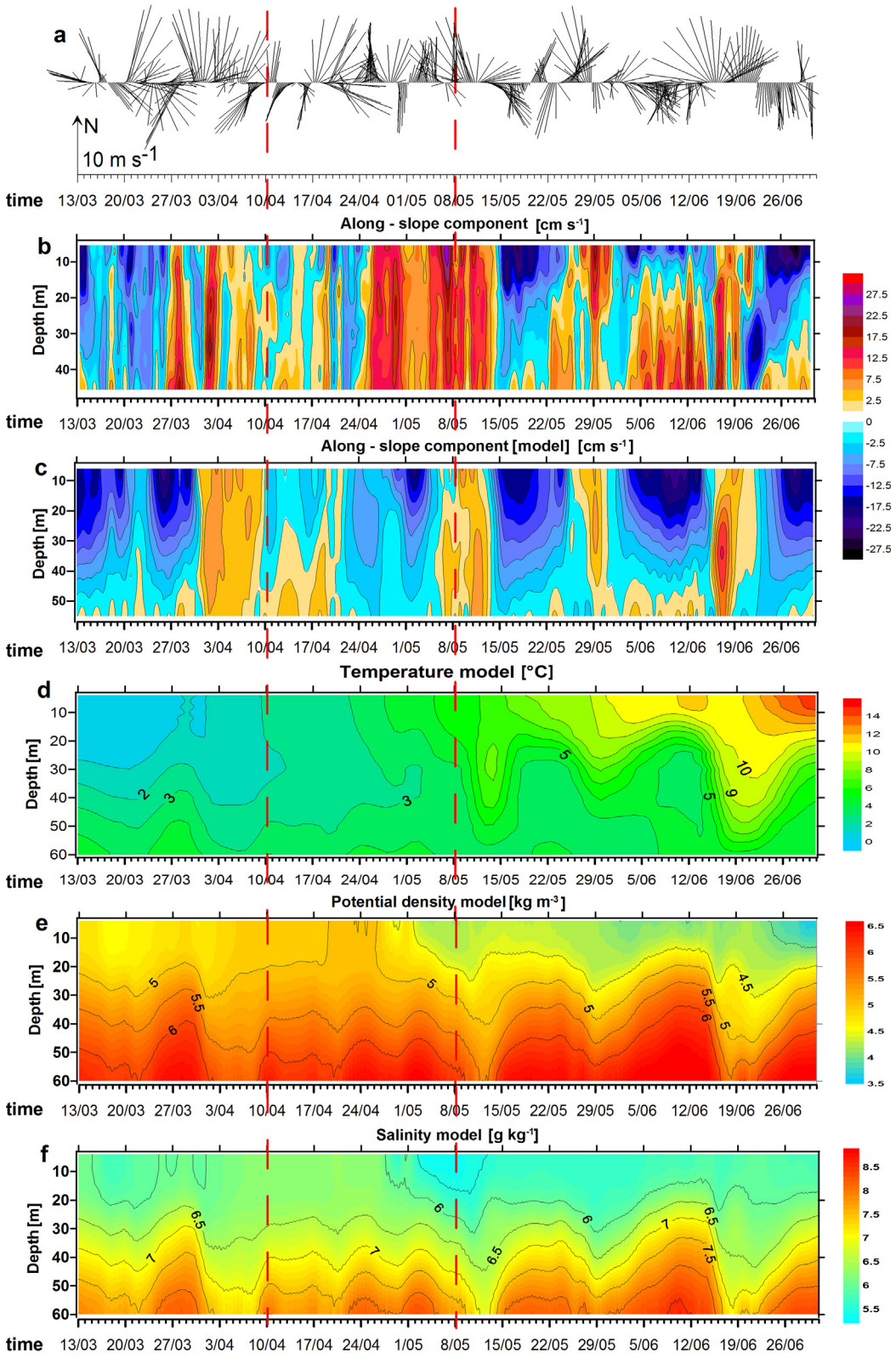

Figure 2 (a) Time series of low-pass filtered wind vectors subsampled every 5 h for visual clarity. An arrow on the time axis shows the scaling of wind vectors. The direction of the arrow approximates the along-coast eastward direction (60° from N). Time series of the low-pass filtered along-isobaths current velocity component in cm s^{-1} from observations (b) and model (c). Positive velocities (red) display the inflow into the gulf (along-isobaths component) or offshore flow (across-isobaths component), and negative velocities (blue) display the opposite flow respectively ((d) and (e)). Time series of the modelled temperature and the potential density respectively. The vertical dashed lines drawn throughout the panels divide the whole period for three sub-periods. (For interpretation of the references to colour in this figure legend, the reader is referred to the web version of this article.)

In the present study, we used the HIROMB current velocity, sea level, sea level gradients and temperature data (1-h time-series) to compare the measurements and to enhance comprehension of the physical processes involved.

3. Results

3.1. Atmospheric forcing

Wind over the area was promoted by the mainly eastward moving atmospheric cyclones of a few days' duration and by the prolonged sedentary anticyclones. Accordingly, the range of hourly wind speeds was wide, covering light to moderate (68% of the whole period), fresh (23%) and strong (9%) wind speeds. Relatively high percentage of fresh and strong winds (>8 m s^{-1}) assumes the inducing of the moderate wind-driven current in the upper layer as well as generation of the coastal up- and downwelling events. Altogether six mainly WSW stronger (>13 m s^{-1}) wind events with the duration of about a day occurred. For example, during the strongest event on 19 April, the WSW wind speeds reached 17 m s^{-1}. The time scale of wind variation was considerably shorter during the first half of observations than within the latter period (see Fig. 2a). The latter was characterised by almost steady wind periods with the duration of 2—7 days.

Unfortunately, our current measurements were not accompanied by the mapping of temperature and salinity. Therefore, to estimate the development of the seasonal vertical stratification, which is an important background condition in the formation of flow structure, we used the courses of air temperature at Pakri and the vertical sea temperature distribution obtained from the model. The winter of 2008/2009 was relatively mild in the Baltic region, which resulted in the practically ice-free western Gulf of Finland. The mean air temperature (January—March) was 1.4°C and slightly higher in the following three weeks in April (3.2°C). After that, the first springtime heat wave with the duration of five days and with maximum temperatures up to ~20°C hit the region. From the beginning of May, the air temperature gradually rose within the limits of interannual variability. The modelled temporal vertical distribution of sea temperature at the measurement site (Fig. 2d) was in accordance with main tendencies in the course of air temperature. The seasonal stratification started to develop at the end of April and by about mid-May, a moderate thermocline was already present. Thus, in accordance with the modelled sea temperature distribution, the whole observation period was divided into three sub-periods — the weak inverse thermal stratification typical of the end of winter season until 10 April, the summer type stratification from 8 May onwards, and the 'transition' period with negligible thermal stratification between them. The transition period was formally defined as the period when the temperature difference between the surface and the bottom layers, either positive or negative, was less than 2°C in absolute value. Note that the modelled density stratification (Fig. 2c) was weakened but hydrostatically stable even during the transition period, obviously due to the increase of salinity with depth (Fig. 2f).

3.2. Variability of low-frequency current

In general, the low-frequency flow along the isobaths was much stronger than the across-isobaths flow during almost the whole observation period (Figs. 2b and 3a). The alternation of shorter or longer periods of eastward or westward (hereinafter in the frame of rotated coordinates) currents indicating inflow into or outflow from the gulf, respectively, was the most common feature of the temporal flow pattern. However, the structure of the low-frequency current was quite different depending on the strength of density stratification.

During the periods of weak density stratification (i.e., until the summer type stratification is established), the current had quasi-barotropic character with some intensification in the upper about 15-m layer (Fig. 2b). As soon as the summer

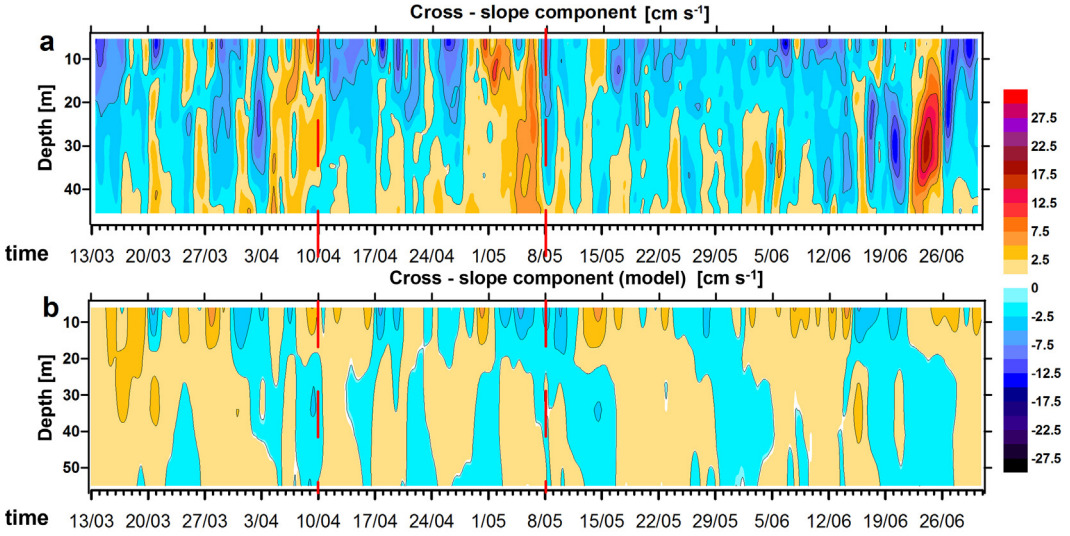

Figure 3 Time series low-pass filtered cross-isobaths current velocity components: (a) observations and (b) model. The vertical dashed lines drawn throughout the panels divide the whole period into three sub-periods.

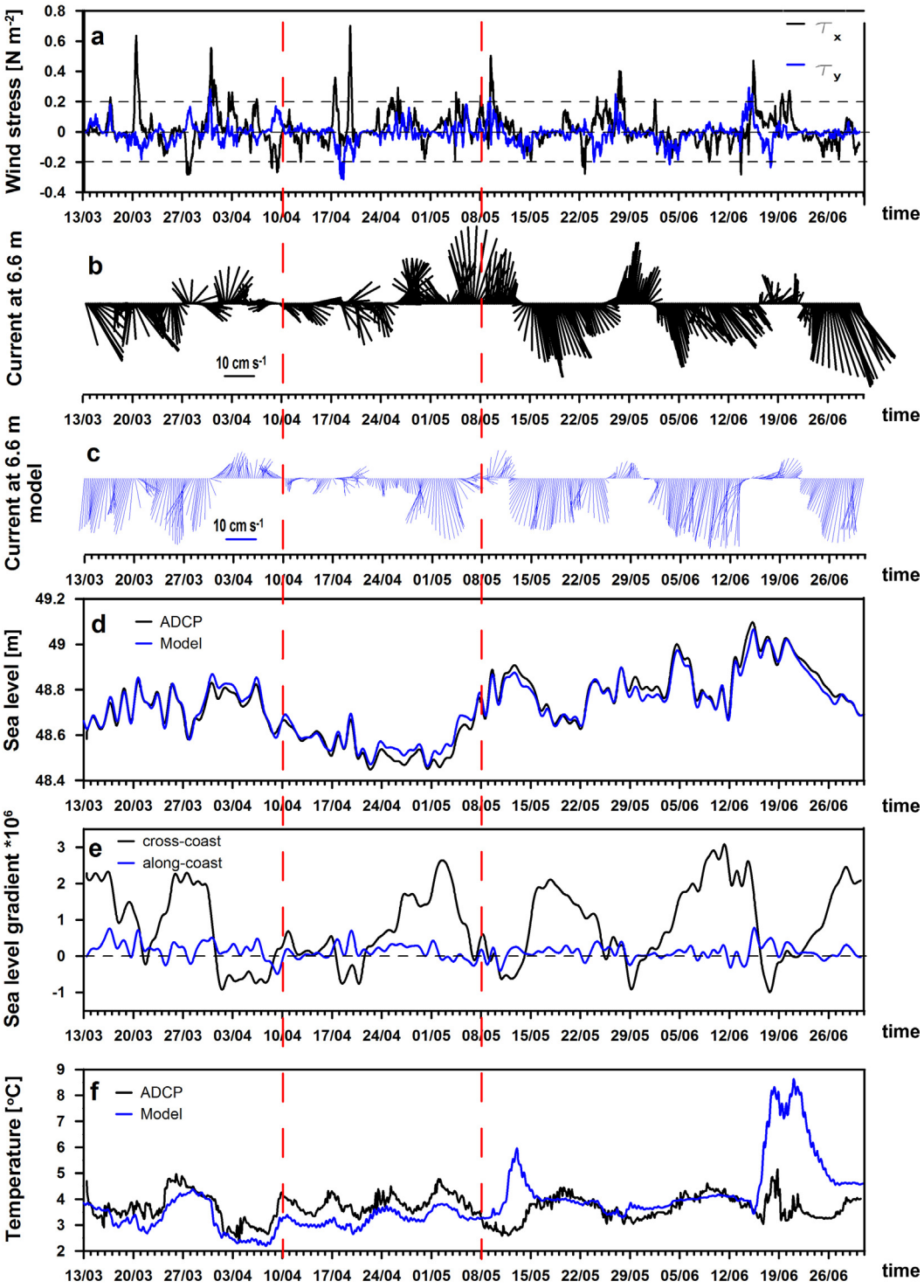

Figure 4 (a) Hourly time series of along-coast (black line) and cross-coast (blue line) wind stress components. ((b) and (c)) Low-pass filtered observed (black line) and modelled (blue line) current vectors at 6.6 m depth (subsampled every 5 h). Straight line on the time axis shows the scaling of current vectors. (d) Low-pass filtered conditional sea level from the ADCP pressure sensor (black line) and from the model (blue line). (e) Low-pass filtered across-isobaths (black line) and along-isobaths (blue line) sea level gradients calculated from the model. (f) Observed (black line) and modelled (blue line) hourly near-bottom temperature. The vertical dashed lines drawn throughout the panels divide the whole period into three sub-periods. (For interpretation of the references to colour in this figure legend, the reader is referred to the web version of this article.)

type stratification is established, the current becomes more baroclinic displaying a two-layer structure for considerable time intervals. Note that the barotropic character was mostly peculiar to the eastward flow when the density stratification weakened due to downwelling. There were periods with minor along-isobaths current component (e.g., 13—15 April), but dominantly the velocities varied around 5—10 cm s^{-1} in both directions. At times, the stronger current in the upper layer compared to that in the layers below was more likely wind-induced, i.e., it reveals a response to the stronger wind events. This was confirmed by the relatively high correlation between the wind stress and the current vectors ($R = 0.39$, lag 2 h) despite the considerable depth (6.6 m) at which the current was measured. For example, the typical current speeds at 6.6 m depth were 6—7 cm s^{-1} on 25 March and 12 April. Corresponding excess of the current speed with respect to 20.6 m depth of ~3 cm s^{-1} was in reasonable compliance with that calculated with the classical Ekman model.

The most stable current, barotropic by character, was observed during the period of 25 April—15 May (Fig. 2b). That kind of flow can be explained by relatively stationary W-SW wind (Fig. 2a) and weak density stratification. The resulting inflow (eastward) was evenly distributed over the whole water column, while the typical along-isobaths current velocities were 10—15 cm s^{-1}. Again, similarly to the previous period, the upper 15-m layer was affected by the stronger winds.

The low-frequency flow within the summer type stratification period was mostly two-layered and its along-isobaths component was usually much stronger than during the weakly stratified period (cf. the left- and right-hand sides of Fig. 2b). The flow was most pronounced in the upper 15-m layer, where intense and about 10-days long outflow events with speeds reaching 30 cm s^{-1} alternated with weaker (up to 20 cm s^{-1}) and shorter inflow events. Such high low-frequency current speeds cannot be explained by the wind-driven current and/or barotropic flow due to across-coast sea level gradients alone. Therefore, considering the prevailingly along-coast oriented (in both directions) background wind pattern (Figs. 2a and 4a), presumably upwelling and downwelling associated baroclinic currents were involved. We will substantiate that by an analysis in Sections 3.3 and 4.1.

Below the seasonal thermocline (depth >15 m), the inflow episodes with different extent from the bottom were characteristic of the summer conditions (Fig. 2b). Surprisingly, these eastward flow episodes took place when the wind was explicitly (except on 16—17 June) from eastern directions (Figs. 2a and 4a). The along-isobaths velocities had an evident tendency to increase towards the bottom, and within the most prominent inflow period (3—14 June) they reached up to 18.5 cm s^{-1}. Besides, a clear oscillating character with periods of about 2—3 days during all episodes is rather unconventional for a current in the deeper layers of the gulf. The origin of such upwind current will be discussed in Section 4.2. The strongest westward flow with maximal speeds exceeding 15 cm s^{-1} at about 30 m depth occurred starting from 20 June. This intensification of the along-isobaths current component and the distribution of the enhanced across-isobath component between the depths of 15 and 40 m (19—26 June) with a sign change (Fig. 3a) are more likely the signatures of an anticyclonic eddy-like structure. The succession of the sign change of both current components reveals that this structure migrated eastward and 'touched' (about a week) our measurement site with its southern periphery. During the rest of the stratified period, the across-isobaths flow component was weak and without firm direction (Fig. 3a).

Finally, permanent, quasi-barotropic undulations of current velocity components with the period of 2—5 days are seen more prominently in the along-isobath component (cf. Figs. 2b and 3a). These undulations are most probably caused by topographic waves (Lilover and Talsepp, 2014).

3.3. Upwelling and downwelling events

Coastal upwelling is usually verified by using the satellite images of the sea surface temperature (SST) or mapping of temperature/salinity fields. In the absence of the latter we explored temporal vertical distribution of the temperature from the model data (Fig. 2d), which revealed qualitatively well the rising (dropping) of thermocline in the study area during easterly (westerly) winds, i.e., supporting occurrence of upwelling (downwelling) events. Because the Gulf of Finland is a narrow basin, an upwelling along one coast is accompanied by a downwelling along the opposite coast. Thus, such a coupled mechanism enables us to conclude the presence of downwelling at the Estonian coast, relying on upwelling signatures at the Finnish coast visible on the satellite SST images. Unfortunately, only a few cloud free SST images covering the periods and the region of our interest were available. These SST images reflected upwelling events on the Estonian coast on 17 May and 29 June and downwelling event on 28 May.

Since upwelling/downwelling events in the southern Gulf of Finland are characterised by a combination of negative/positive along-isobath wind and current pulses and rising/dropping of temperature contours, Figs. 2 and 3 enable clear identification of four upwelling events (23—30 March, 14—24 May, 1—14 June, and 21—30 June), and four downwelling events (31 March—7 April, 8—13 May, 24—30 May, and 15—20 June). Note that the first event of upwelling and downwelling took place during the period of inverse thermal stratification at the end of winter season, while the next three were observed during the period of summer type thermal stratification. Since at the upwelling observed during the period of inverse thermal stratification, the layer of sloping temperature/potential density, 15—45 m, displays a considerable value of the vertical gradient of along-isobath current velocity, we can suggest that the flow, despite a weakened density stratification, is baroclinic. Upwelling/downwelling events during the transition period were not identified because the period under consideration is almost thermally unstratified when the rising/dropping of temperature contours cannot be considered as a signature of upwelling/downwelling processes.

3.4. Comparison with the model

In general, the time series of the observed and modelled vertical distributions of along-isobath current velocity (Fig. 2b and c) display well coordinated intervals of eastward and westward flow in the upper layer. An exception is the

period of 25 April—14 May, which was the longest interval of eastward flow recorded by the ADCP measurements while the model showed the westward transport before 6 May. Unfortunately we could not explain this discrepancy and will leave the issue open. Due to the discrepancy, correlation of the measured and modelled along-isobath current on 6.6 m level (see Fig. 4b and c) was negative for the transition period (−0.39). For the inverse thermal stratification period, the summer-type stratification period, and the whole period of 13 March—30 June, correlation of the measured and modelled along-isobath current on 6.6 m level was positive and relatively high (0.61, 0.52, and 0.82, respectively).

Correlation of the measured and modelled cross-isobath current on 6.6 m level was much lower (0.16 for the whole period). In the deep layers, correlation between the observed and modelled velocities, both along- and cross-isobath, does not exceed 0.2—0.3.

Despite the low correlation of the measured and modelled velocities in the deep layer, a surprisingly high correlation was found between the measured and modelled temperatures in the bottom layer (Fig. 4f): the measured and modelled time series of 44.6 m temperature display almost coherent changes during the whole period of observations except for relatively short intervals of 12—14 May and 17—22 June when the modelled temperature was considerably higher than the measured one. In accordance with Fig. 2b—d, these intervals correspond to well-pronounced downwelling events, when the modelled thermocline deepens to the depth of about 50 m, which results in an excessive increase of the modelled near-bottom temperature. Apart from these intervals, some increase of both the measured and modelled near-bottom temperature is observed during upwelling events, which is explained by the features of typical cross-isobath circulation, when the cross-isobath flow in the near-bottom (near-surface) layer is directed onshore (offshore). With regard to the inverse temperature stratification, the onshore flow in the near-bottom layer results in the increase of the near-bottom temperature. The correlation coefficients between the measured and modelled near-bottom temperature was 0.85, 0.79 and 0.08 for the inverse thermal stratification, transition and summer type stratification periods, respectively. Drastic decrease of correlation in the summer type stratification period is obviously caused by the excessive increase of modelled near-bottom temperature during 12—14 May and 17—22 June downwelling events.

Correlation between the measured and modelled sea level (see Fig. 4d) was extremely high (0.99 for the whole period), which is not surprising — state-of-the-art models are known for excellent prediction of sea level changes. Correlation between the measured (modelled) 6.6 m along-isobath velocity and the modelled cross-isobath sea level gradient (see Fig. 4b, c and e) was −0.45 (−0.86). Note that in the ideal case of a geostrophically-balanced flow, correlation between the along-isobath velocity at the sea surface and the cross-isobath sea level gradient should be −1.

Finally, we may conclude that the quasi-barotropic oscillations of the velocity current with a 2—5 day period, supposedly caused by topography waves (Lilover and Talsepp, 2014), are less pronounced in the model than in the measurements (cf. Fig. 2b and c, Fig. 3a and b).

4. Discussion and conclusions

The observed low-frequency flow appeared very complex and was strongly dependent on the stratification. Under weak density stratified conditions, the current was almost barotropic whereas at times some intensification occurred in the upper layer due to stronger wind pulses. These results are comparable to observations published by Liblik et al. (2013). The seasonal stratification in combination with wind conditions caused different flow patterns in the upper and deeper layers. In the following, some aspects and nature of the observed currents are discussed.

4.1. Position of upwelling and downwelling related front/current

Taking into account that the eastward flow occupied the whole water column during downwelling events within the summer type stratification period (see Fig. 2b and c), it may be suggested that the ADCP measurements were performed at the onshore periphery of the jet-like current associated with downwelling/upwelling (Zhurbas et al., 2006). Therefore, the displacements of the upwelling and downwelling front from the coast were estimated. A non-linear two-layer model with impulsively exerted wind stress by Csanady (1977) enables us to find the offshore distance (y_0) where the pycnocline surfaces as

$$y_0 = \frac{I}{f\rho_0 h_1}\frac{h_2}{h_1+h_2} - R, \tag{1}$$

where h_1 and h_2 are the top and bottom layer thicknesses, respectively, I is the cumulative wind stress, $R = f^{-1}[g'h_1h_2/(h_1+h_2)]^{1/2}$ is the baroclinic radius of deformation, f is the Coriolis parameter, $g' = g(\Delta\rho_1/\rho_0)$ is the reduced gravity, g is the gravitation acceleration (9.8 m s^{-2}), ρ_0 is the reference density (1000 kg m^{-3}), and $\Delta\rho_1$ is the density difference between the two layers. Taking h_1 = 12 m and h_2 = 48 m (means average cross-gulf depth of 60 m), and assuming $\Delta\rho_1 \approx \Delta\rho$ (=0.6 kg m^{-3}), formula (1) gives the outcrop of pycnocline 10.4 km from the coast for the upwelling event of 21—30 June (I = 0.27 N m^{-2} d). Note that for the event of 14—24 May (I = 0.15 N m^{-2} d, $\Delta\rho_1$ = 0.25 kg m^{-3}), y_0 = 5.6 km, i.e., practically the distance of the observation site. The offshore displacement of the downwelling front (y_1) according to Austin and Lentz (2002) is scaled as

$$y_1 = \sqrt{\frac{2I}{f\rho_0\beta'}}, \tag{2}$$

where β is the bottom slope. Taking β = 0.007 as characteristic of our study area and I = 0.60 N m^{-2} d for the downwelling event of 15—20 June, formula (2) gives y_1 = 10.9 km.

Thus, the estimates of the displacement of the front (centre) from the coast for events of 15—20 June and 21—30 June are both about 10 km. The width of the upwelling/downwelling jet is expected to be a few baroclinic Rossby deformation radii. In the Gulf of Finland the deformation radius is 2—4 km (Alenius et al., 2003) and correspondingly the width of the jet is around 10 km. However, the widths obtained from the model data on the north-south oriented leg (see Fig. 1b) are 15—17 km, thus too large obviously

because of a 'smoothing' effect of the model. On the other hand, the only available (to our knowledge) observational estimate of the width, 8—12 km, for the downwelling jet at the entrance area to the gulf (Laanemets et al., 2005) coincides well with the scaled estimate. Therefore, considering the scaled width of the jet and estimated jet's displacement from the coast, it is highly plausible that our data (about 6 km from the coast) originate from the southern periphery of the jet.

4.2. Upwind current below the thermocline

Next, we examine the eastward current episodes below the seasonal thermocline, which were observed during the easterly winds (Fig. 3a and b). Such an upwind flow is a commonly known phenomenon from the studies focused on the elongated basins and estuaries since the 1970s (e.g., Csanady, 1973), and its essence is as follows. The along-axis wind causes a cross-shore Ekman transport in the upper layers and, as a result, the sea level rises on the right-hand coast looking downwind and drops on the left-hand coast. Due to the corresponding barotropic pressure gradient forces, the downwind jet-like current at both coasts is produced. Besides, the Ekman transport generates upwelling and downwelling at the left- and right-hand coasts, respectively. Therefore, in the presence of stratification, the associated baroclinic downwind current component enhances the jets at both coasts. The transport by these strong downwind jets gives rise to the upwind flow in the central area of the basin, which was predicted by numerous analytical as well as numerical models. However, the Coriolis force (important for larger basins) has been included in the analytical models only since the last decade. The solutions of 'pure' barotropic models (e.g., Winant, 2004) as well as of more general models including baroclinic forcing (e.g., Reyes-Hernandez and Valle-Levinson, 2010) reveal well a bottom intensified upwind flow flanked by the surface intensified downwind jets along the coasts and the sensitivity of this flow pattern on the across-estuary depth variations.

According to our study (at the coastal area of the elongated estuary-like gulf), the most pronounced upwind (eastward) current event occurred on 3—14 June (Fig. 2b) and as was shown in the previous section, it even affected the downwind flow in the upper layer. The specific features of the current within this period are the intensification towards the bottom and relatively close relation with variations of the along-coast component of wind stress (Fig. 5). The current speed gradually increased down to the depth of 42.6 m and most likely decreased underneath ('untouchable' by the ADCP) due to the bottom stress. The along-isobaths current speeds (low-frequency) were relatively high: 10.6 cm s^{-1} as average and 18.5 cm s^{-1} as maximum (both at 42.6 m depth). Such current speeds are comparable with results presented by Liblik and Lips (2012) and other observations in larger estuaries. For example, subtidal upwind mean inflow speeds up to 19 cm s^{-1} at the entrance to Long Island Sound (Whitney and Codiga, 2011) and in the range of 10—20 cm s^{-1} in the southern (deep) entrance area to Chesapeake Bay (Valle-Levinson et al., 2001, their Fig. 10b and d) were reported. Earlier observations of the deep eastward-directed current during seaward wind in the Gulf of Finland were revealed by Lips et al. (2009) and Liblik et al. (2013). Here we mention that the upwind flow predicted by the HIROMB model was underestimated (mean and maximum speeds of 2.3 and 7.5 cm s^{-1}, respectively at 40 m grid horizon) obviously because of too sparse grid resolution below the seasonal thermocline.

The upwind current was observed relatively close to the coast (6 km), nevertheless above the 50-m bottom. Therefore, it is likely that the flow event occupied at least most of the southern portion of the gulf cross-section (below thermocline). This complies with other observations (e.g., Whitney and Codiga, 2011) as well as predictions of models with stratification (e.g., Reyes-Hernandez and Valle-Levinson, 2010). The latter study also exposed a substantial asymmetry of the lateral distribution of upwind flow (result of possible influence of the Earth's rotation), i.e., a core of the flow was shifted towards the right coast (looking downstream) in the presence of weak and moderate winds. Thus, the relatively high current speeds at our site might in some respects prove the predicted asymmetry.

The reason why the upwind flow developed so strong and lasted over a 10-day period lies obviously in the favourable wind conditions. The recurrent westward, along-coast wind stress component pulses with maximum magnitudes of 0.1—0.25 N m^{-2} dominated (Fig. 5), which was sufficient

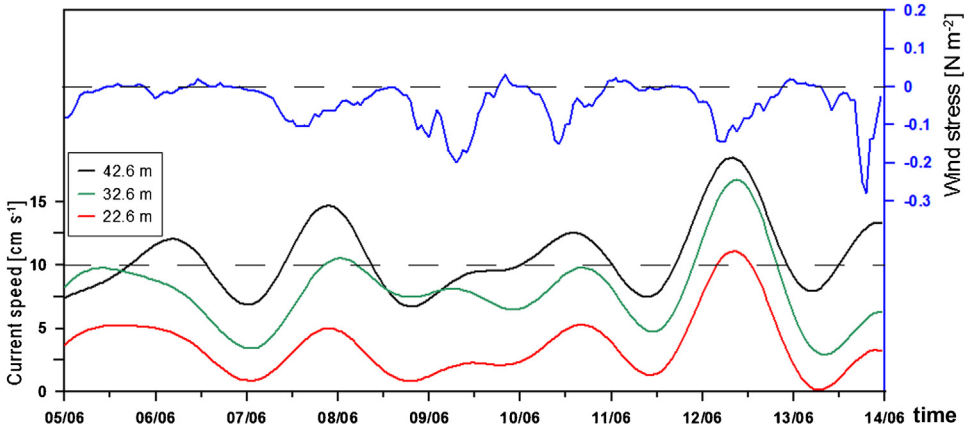

Figure 5 Time series of the low-pass filtered along-isobath current velocity component at 22.6, 32.6, and 42.6 m and the along-isobath wind stress component for the period of 5—14/06.

for the maintenance of the above proposed circulation in the elongated gulf. Moreover, variations of the along-coast wind stress component and correspondingly the changes of the cross-coast sea level gradients ($r = -0.46$, 3 h lag) probably caused the variations in the strength of the eastward current. It is clearly seen that the current strengthened shortly after the wind stress magnitude began to increase and weakened when the wind stress was negligible (Fig. 5). The barotropic response is also confirmed by a significant correlation ($r = -0.28$, 2 h lag) between the components of the cross-coast sea level gradient and the along-isobaths current (at 42.6 m depth). Other eastward, bottom intensified flow events related to periods of 16–25 May and onward from 23 June were considerably weaker and embraced mainly 15–20 m layer above the bottom (Fig. 3b). The upwind current during the period of 16–19 May was very weak, which is likely because of the almost decayed wind (Fig. 4a). However, strong easterly wind pulse on 22 May efficiently enhanced the upwind flow. The full development of the upwind flow event related to period from 23 June onward stayed out of the observation window, but in the initial stage the flow might have been somewhat affected by the eddy-like structure. Thus, at the southern coast of the gulf, the eastward (upwind) flow seems to be a common phenomenon during easterly wind periods, while being very sensitive to the short-term variations of the wind.

4.3. Long-term mean flow

Finally, the mean currents over the whole observation period and those obtained from different multiyear numerical model simulations in the western Gulf of Finland are compared. The five-year forecast by Andrejev et al. (2004) and the three-year forecast (HIROMB model) by Elken et al. (2011) both expose well a cyclonic circulation pattern in the gulf, i.e., a strong westward Finnish Coastal Current and in general eastward flow over almost the whole water column in the southern gulf. Relying on the progressive vector plots, our data indicate a substantially different current succession in the upper layer (Fig. 6a) and deeper layers (Fig. 6b). In the latter, prevailingly along-isobaths inflow occurs during the whole observation period. At the same time, in the upper layer outflow dominates despite stratification conditions, although the flow is considerably inclined toward the coast. Exceptionally, the flow is eastward during the transition period, thus similar to the flow in the deeper layer. In the upper layer, the mean current vector over a 3.5-month period has along- and across-isobaths components of -2.0 and $-2.9\ \mathrm{cm\ s^{-1}}$, respectively. Such mean flows are mostly composed of the westward flow during the inversely thermal stratification period as well as the enhanced westward flow during upwelling events. In the deeper layers the mean current with components of 1.1 and $-0.3\ \mathrm{cm\ s^{-1}}$ for along- and across-isobaths directions, respectively, is weaker, and contributed mainly by the stronger barotropic flow within the transition period and the eastward upwind flow events.

Thus, our data reveal the expected mean flow towards the inner gulf only in the deeper layers. For the upper layer the existing models give contrary long-term current directions in the surrounding of the observation site. The mean (1987–1992) flow with speeds $\sim 5\ \mathrm{cm\ s^{-1}}$ is eastward (Andrejev et al., 2004, their Fig. 8) and therefore complies with the understanding of the general cyclonic circulation in the gulf. On the other hand, the mean (2006–2008) westward flow of $\sim 3\ \mathrm{cm\ s^{-1}}$ as a southern part of relatively large anticyclonic circulation cell (Elken et al., 2011, their Fig. 2) fits well with our estimate. Accordingly, the inflow of open Baltic waters at this longitude takes place over the deepest part of the gulf. A similar result was also obtained using the same model for years 2010–2011 (Lagemaa, 2012, Fig. 7). Our findings contradict the results of earlier coastal numerical circulation, but fit well with recent studies. Therefore, it is highly possible that the processes described in this study will mainly cause the modelled long-term westward flow over the slope. A precondition for such speculation is the timing of our

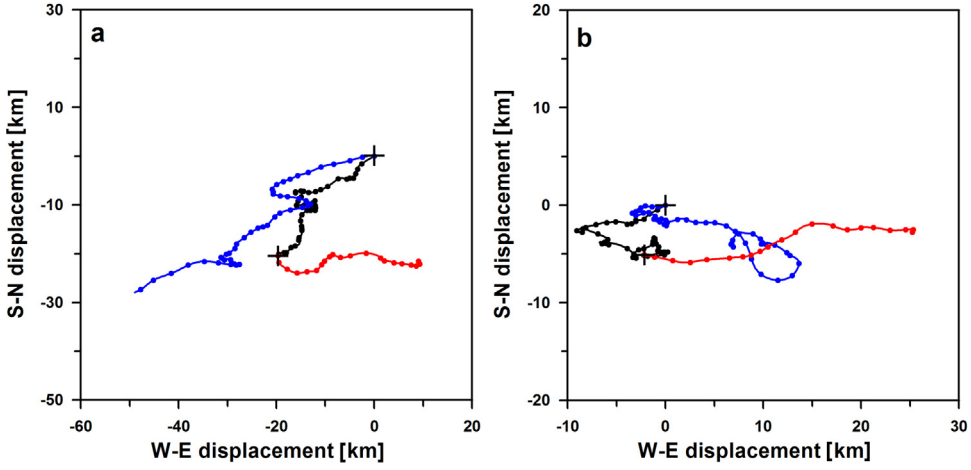

Figure 6 Progressive vector diagrams of low-frequency average current over 6.6–8.6 m layer (a) and 20.6–42.6 m layer (b). Black (red) lines and dots indicate inversely thermal stratification (transition) periods. Blue lines and dots show the summer type stratification period. Dots on the curves are shown after each day. The progressive vector diagram is restarted between the periods; the plus marks the starting point. (For interpretation of the references to colour in this figure legend, the reader is referred to the web version of this article.)

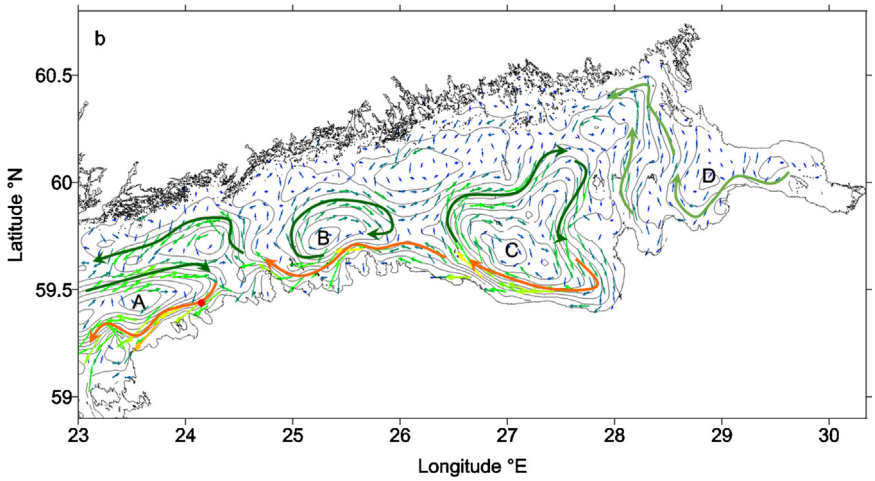

Figure 7 Reprint from Lagemaa (2012) with additional illustrations enhancing the circulation patterns. The location of the bottom-mounted ADCP is shown by a red dot. (For interpretation of the references to colour in this figure legend, the reader is referred to the web version of this article.)

observations, i.e., it partly covers unstratified as well as stratified seasons of the sea. As was shown, the observed westward mean flow results largely from the jet-like currents related to upwelling. However, upwelling at the southern coast of the gulf is not a very common process as follows from the 20-year (1990—2009) statistical analysis of summer satellite SST images, which expose the frequency of occurrence only up to 12% in June (Lehmann et al., 2012). In spite of rare occurrences of upwelling events in summer, the contribution of related jets (high speeds and duration of about a week) to the long-term mean current may be substantial. The same holds also for the weakly density stratified season when relatively strong westward barotropic currents due to easterly wind impulses may occur. Hence, the mean westward flow in the upper layer (observed and modelled by the HIROMB) at our observation site reflects probably a local coarse-scale feature of the long-term general circulation.

To summarise, our results show that even single point current velocity measurements with a combination of selected data from a relatively coarse numerical circulation model enable acquisition of valuable knowledge about different coastal processes and their contribution to the overall circulation. However, the present understanding of currents over the slopes is still clearly inadequate. Therefore, long-time current measurements together with frequent density mapping covering other seasons and areas of the Gulf of Finland are likely to be in the focus of research in the coming years.

Acknowledgements

We express our gratitude to Viktor Zhurbas for fruitful consultations. We are grateful to Kaimo Vahter for assistance in the deployment of the ADCP and to Rivo Uiboupin for providing satellite SST images. The model data were kindly provided by the Swedish Meteorological Institute under cooperation within BOOS (Baltic Operational Oceanographic System) and HIROMB.

References

Alenius, P., Myrberg, K., Nekrassov, A., 1998. Physical oceanography of the Gulf of Finland: a review. Boreal Environ. Res. 3, 97—125.

Alenius, P., Nekrasov, A., Myrberg, K., 2003. Variability of the baroclinic Rossby radius in the Gulf of Finland. Cont. Shelf Res. 23, 563—573.

Andrejev, O., Myrberg, K., Alenius, P., Lundberg, P.A., 2004. Mean circulation and water exchange in the Gulf of Finland — a study based on three-dimensional modeling. Boreal Environ. Res. 9, 1—16.

Austin, J.A., Lentz, S.J., 2002. The inner shelf response to wind-driven upwelling and downwelling. J. Phys. Oceanogr. 32, 2171—2193.

Book, J.W., Perkins, H., Signell, R.P., Wimbush, M., 2007. The Adriatic Circulation Experiment winter 2002/2003 mooring data report: A case study in ADCP data processing. Memo. Rep. NRL/MR/7330-07-8999. U.S. Naval Res. Lab., Stennis Space Center, MS.

Butterworth, S., 1930. On the theory of filter amplifiers. Exp. Wireless Wireless Eng. 7, 536—541.

Csanady, G.T., 1973. Wind-induced barotropic motions in long lakes. J. Phys. Oceanogr. 3, 429—438.

Csanady, G.T., 1977. Intermittent "full" upwelling in Lake Ontario. J. Geophys. Res. 82, 397—419.

Cushman-Roisin, B., Gačić, M., Poulain, P.-M., Artegiani, A. (Eds.), 2001. Physical Oceanography of the Adriatic Sea: Past, Present, and Future. Kluwer Academic Publisher, Dordrecht, p. 304.

Elken, J., Nõmm, M., Lagemaa, P., 2011. Circulation patterns in the Gulf of Finland derived from the EOF analysis of model result. Boreal Environ. Res. 16, 84—102.

Elken, J., Raudsepp, U., Lips, U., 2003. On the estuarine transport reversal in deep layers of the Gulf of Finland. J. Sea Res. 49, 267—274.

Funkquist, L., 2001. HIROMB, an operational eddy-resolving model for the Baltic Sea. Bull. Maritime Inst. Gdansk 28, 7—16.

Gästgifvars, M., Müller-Navarra, S., Funkquist, L., Huess, V., 2008. Performance of operational systems with respect to water level forecasts in the Gulf of Finland. Ocean Dyn. 58, 139—153.

Huthnance, J.M., 1995. Circulation, exchange and water masses at the ocean margin: the role of physical processes at the shelf edge. Prog. Oceanogr. 35, 353—431.

Keevallik, S., Männik, A., Hinnov, J., 2010. Comparison of HIRLAM wind data with measurements at Estonian coastal meteorological stations. Estonian J. Earth Sci. 59 (1), 90—99.

Keevallik, S., Soomere, T., 2010. Towards quantifying variations in wind parameters across the Gulf of Finland. Estonian J. Earth Sci. 59, 288—297.

Laanemets, J., Pavelson, J., Lips, U., Kononen, K., 2005. Downwelling related mesoscale motions at the entrance to the Gulf of Finland: observations and diagnosis. Oceanol. Hydrobiol. Stud. 34, 15—36.

Lagemaa, P., 2012. Operational forecasting in Estonian marine waters. (PhD Thesis). Tallinn Univ. Technol., TUT Press, 45.

Lagemaa, P., Suhhova, I., Nõmm, M., Pavelson, J., Elken, J., 2010. Comparison of current simulations by the state-of-the-art operational models in the Gulf of Finland with ADCP measurements. In: 4th US/EU Baltic Symp., 24—27 August 2010, IEEE Conf. Proc, Riga, http://dx.doi.org/10.1109/BALTIC.2010.5621656.

Lehmann, A., Myrberg, K., Höflich, K., 2012. A statistical approach to coastal upwelling in the Baltic Sea based on the analysis of satellite data for 1990—2009. Oceanologia 54, 369—393.

Liblik, T., Laanemets, J., Raudsepp, U., Elken, J., Suhhova, I., 2013. Estuarine circulation reversals and related rapid changes in winter near-bottom oxygen conditions in the Gulf of Finland, Baltic Sea. Ocean Sci. 10, 727—762.

Liblik, T., Lips, U., 2011. Characteristics and variability of the vertical thermohaline structure in the Gulf of Finland in summer. Boreal Environ. Res. 16A, 73—83.

Liblik, T., Lips, U., 2012. Variability of synoptic-scale quasi-stationary thermohaline stratification patterns in the Gulf of Finland in summer 2009. Ocean Sci. 8, 603—614.

Lilover, M., Pavelson, J., Köuts, T., 2011. Wind forced currents over the shallow Naissaar Bank in the Gulf of Finland. Boreal Environ. Res. 16, 164—174.

Lilover, M.-J., Talsepp, L., 2014. On the vertical structure of the low-frequency oscillations of currents in the Gulf of Finland. In: Baltic International Symposium (BALTIC), 2014 IEEE/OES. 1—6.

Lips, I., Lips, U., Liblik, T., 2009. Consequences of coastal upwelling events on physical and chemical patterns in the central Gulf of Finland. Cont. Shelf Res. 1836—1847.

Rao, Y.R., Schwab, D.J., 2007. Transport and mixing between the coastal and offshore waters in the Great Lakes: a review. J. Great Lakes Res. 33, 202—218.

Reyes-Hernandez, C., Valle-Levinson, A., 2010. Wind modifications to density-driven flows in semienclosed rotating basins. J. Phys. Oceanogr. 40, 1473—1487.

Soomere, T., Keevalik, S., 2003. Directional and extreme wind properties in the Gulf of Finland. Proc. Estonian Acad. Sci. Eng. 9, 73—90.

Soomere, T., Myrberg, K., Leppäranta, M., Nekrasov, A., 2008. The progress in knowledge of physical oceanography of the Gulf of Finland: a review for 1997—2007. Oceanologia 50, 287—362.

Stipa, T., 2004. Baroclinic adjustment in the Finnish coastal current. Tellus 56A, 79—87.

Suursaar, Ü., Aps, R., 2007. Spatio-temporal variations in hydrophysical and -chemical parameters during a major upwelling event off the southern coast of the Gulf of Finland in summer 2006. Oceanologia 49, 209—228.

Thuillier., R.H., Lappe, U.O., 1964. Wind and temperature profile characteristics from observations on a 1400 ft tower. J. Appl. Meteor. 3, 299—306.

Valle-Levinson, A., Wong, K.-C., Bosley, K.T., 2001. Observations of the wind-induced exchange at the entrance to Chesapeake Bay. J. Mar. Res. 59, 391—416.

Whitney, M.M., Codiga, D.L., 2011. Response of a large stratified estuary to wind events: observations, simulations, and theory for Long Island Sound. J. Phys. Oceanogr. 41, 1308—1327.

Winant, C.D., 2004. Three-dimensional wind-driven flow in an elongated, rotating basin. J. Phys. Oceanogr. 34, 462—476.

Zhurbas, V., Laanemets, J., Vahtera, E., 2008. Modeling of the mesoscale structure of coupled upwelling/downwelling events and the related input of nutrients to the upper mixed layer in the Gulf of Finland, Baltic Sea. J. Geophys. Res. Oceans C113, 1—8.

Zhurbas, V., Oh, I.S., Park, T., 2006. Formation and decay of a longshore baroclinic jet associated with transient coastal upwelling and downwelling: a numerical study with applications to the Baltic Sea. J. Geophys. Res. Oceans 111, C04014, http://dx.doi.org/10.1029/2005JC003079.